POLYTECHNIC UNIVERSITY OF MILANO

Department of Aerospace Science and Technology (DAER)

THERMAL ADJOINT OPTIMIZATION OF ELECTRIC PROPULSION SYSTEMS FOR AEROSPACE

Author of the project:
Manuel Monfort Muñoz

Qualification:
Degree in Aerospace Engineering. Intensification in Propulsion.

Director of the work:
Federico Piscaglia

Co-director of the work:
Emanuele Gallorini

Milano, June 2023

Index

Index of Figures

Index of Tables

Nomenclature

Latin letters

b	Vector of design variables
BC^P	Adjoint boundary condition for mass conservation equation
BC^u	Adjoint boundary condition for momentum equation
BC^T	Adjoint boundary condition for energy equation
D	Thermal diffusivity
G	Sensitivity
J	Cost function
J_1	Objective function referred to the mechanical power dissipated by the fluid through the boundaries
J_2	Objective function referred to the net thermal power recoverable from the domain
$\overline{J_1}$	Normalized function of J_1
$\overline{J_2}$	Normalized function of J_2
L	Augmented objective function
p	Pressure
q	Adjoint pressure
R	Set of governing equations for the problem
R^p	Mass conservation equation
R^u	Momentum conservation equation
R^T	Energy conservation equation
R^a	Set of adjoint equations
R^q	Adjoint mass conservation equation
R^v	Adjoint momentum conservation equation
R^{Ta}	Adjoint energy conservation equation
T_a	Adjoint temperature
u	Velocity
v	Adjoint velocity
v_n	Normal component of the adjoint velocity
v_t	Tangential component of the adjoint velocity
w	Weighting factor
w_1	Specific weighting factor for J_1
w_2	Specific weighting factor for J_2

Greek letters

α	Porosity
η	Pseudo density
λ	Set of Lagrangian multipliers
ν	Kinematic viscosity
ρ	Density
∇	Nabla operator
$\nabla_{\|\|}$	In-plane component of the Nabla operator

Super indices

*	Referred to a zero gradient BC
**	Referred to an adjoint type BC

1. Introduction

1.1. Introduction

As industrial systems become more complex and sophisticated, efficient solutions to thermal fluid concerns are necessary. The use of electric motors in the aerospace and automotive sectors, for example, has lately garnered attention for technological and environmental reasons. To enhance heat and mass transfer operations, properly disperse the vast amounts of waste heat in sophisticated avionics, and optimize energy utilization, improving propulsion and cooling systems is critical. Pressure drop in cooling systems must be avoided owing to heat transfer difficulties in order to restrict the pumping power given to the working fluid, which will eventually be dissipated due to its viscosity. By reducing the pressure drop, the pump needed for the cooling systems will be eventually smaller, reducing weight which is crucial for an aircraft. Thermal system parametric design optimization is related with various structural and physical parameters of high complexity; a trial-and-error technique for the general design approach is typically time-consuming and does not assure the best design. As a result, optimization techniques like shape optimization (SO) and topology optimization (TO) are commonly used.

Topology Optimization is one of the methods that may make a breakthrough beyond the existing parametric design procedures. Topology Optimization was proposed by Bendsoe and Kikuchi [2] in 1988. Then, Bendsoe and Sigmud gave a systematic introduction of this technique [3]. However, for a long time, TO was only applied in structure mechanics design such as bridge construction and buildings. It took more than 10 years for this elegant concept to enter the research field of fluid dynamics. It was in 2013, when Kontoleontos [4] performed an adjoint based constrained topology for viscous flows concerning heat transfer which is the one of interest for this research.

Topology optimization is a mathematical technique used to optimize the arrangement of materials within a given design space to meet specific loads, boundary conditions, and restrictions. This is achieved by adding solid material into the computational domain, thereby altering the domain's topology to optimize flow characteristics. Shape optimization, on the other hand, involves updating the boundary shape of the domain by parameterizing the borders and adjusting specific parameters until the desired shape is attained. Both ways have the same aim in common, which is basically to minimize an objective function while complying with the given constraints. Topology optimization is particularly suitable for generating initial design concepts that require significant modifications of the computational domain, making it a preferred optimization method for this study.

The conventional topology optimization formulation uses a finite element method (FEM) to evaluate the design performance. Several methods have been used to optimize topology optimization problems, such as heuristic (simulated annealing, genetic algorithms, etc.) and gradient-based algorithms. However, due to the typically large number of control variables, gradient-based methods are commonly favoured for most applications. Adjoint equations can be solved using two common strategies, namely the continuous and discrete adjoint methods. This work employs the continuous adjoint method, which involves deriving and then discretizing the adjoint equations. In contrast, the discrete adjoint method directly derives adjoint equations from the algebraic equations obtained from discretizing the original problem.

The research is carried out in the open-source software called OpenFOAM implemented with an incompressible, single phase, multi-dimensional Finite Volume solver. However, the design and analysis of the solver set up deployed in OpenFOAM is beyond the scope of this paper, which is mainly focused on the post-processing of the simulations performed in the software to evaluate the results and perform several parametric analyses on specific variables to evaluate its impact on the results.

1.2. Goals and highlights

In recent years, the aerospace industry has seen a significant increase in the use of electric propulsion systems. These systems have the potential to be more thermally efficient than traditional propulsion systems, but they also generate a lot of heat during operation. As a result, it's crucial to have effective cooling systems in place to ensure that the electric propulsion systems can operate at peak efficiency.

The cooling system under investigation aims to efficiently dissipate heat from a given process or device while minimizing the mechanical power dissipated by the boundaries. The primary objective of this research is to evaluate the impact of specific variables on the performance of the cooling system, with the purpose of gaining insights into the influence of these variables on the cooling system's thermal and mechanical performance, ultimately leading to the optimization of cooling system design and operation. The analysis will encompass the effects of parameters such as weighting factors, interpolation methods, filtering techniques, and other relevant factors. By examining the interplay between these variables and the resulting system behaviour, valuable insights can be obtained to guide the development and improvement of efficient cooling systems. To address the research objectives, this study will begin by providing an overview of the theoretical framework behind the adjoint optimization solver theory. Understanding the principles and concepts of the adjoint optimization approach is crucial for accurately assessing and interpreting the simulation results. Following a comprehensive understanding of the theory, the study will proceed to analyse the results obtained from the computational simulations, investigating the impact of various variables on the cooling system's performance.

On the other hand, some of the main highlights of the solver used will now be presented. A semi-implicit method for pressure linked equations (SIMPLE) [6] is applied to couple pressure and velocity in the primal and in the adjoint problem. Moreover, a density-based approach for the optimization problem is combined with the Rational Approximation of Material Properties (RAMP) method [7] to model the porosity and material properties between the fluid and the solid. Finally, sensitivity is computed by solving the adjoint equations and used with the Method of Moving Asymptotes [5] to update the design variables.

2. The continuous Adjoint method for topology optimization

2.1. Multi-objective optimization

Optimization refers to the process of finding the best possible solution to a problem out of all possible solutions. It involves identifying a set of variables that can be adjusted within a given set of constraints (expressed as R) to achieve the desired outcome, usually measured by a particular objective function (J). The objective function is a mathematical representation of the goal or target to be achieved, which can be maximized or minimized depending on the nature of the problem. It is now crucial to introduce the design (b) and state variables (x). Design variables are the parameters that can be adjusted during the optimization to achieve a desired outcome. In other words, they are the decision variables that are within the control of the designer or engineer. State variables, on the other hand, are the variables that describe the current state or condition of the system being optimized.

For application of optimization, one could desire to minimize more than a single objective function; therefore, the new goal is to find a set of solutions that represent the best possible trade-offs among two or more competing objectives. Hence, J can be defined as a linear combination of several objective functions (J_i):

$$J = \sum_{i=1}^{n} a_i J_i \tag{1}$$

If all this is transferred to fluid mechanics, the state variables must satisfy (for steady, incompressible flows including heat transfer) three constraints: mass conservation, momentum and energy balance (see Equation 2). Additional constraints can be added depending on the problem formulation.

$$\begin{gathered} \nabla \cdot u = 0 \\ (u \cdot \nabla)\, u + \nabla p - \nabla \cdot (\nu\, \nabla u) = 0 \\ \rho\, c_p (u \cdot \nabla)\, T - \lambda \nabla^2 T + \phi = 0 \end{gathered} \tag{2}$$

The formulation of the problem changes depending on the choice of the design variables and the solution algorithm. Thus, in terms of the design variables chosen, we can opt for a shape optimization (SO)or a topology optimization (TO). On the other hand, another important aspect is the type of solution algorithm used, which can be classified into two main groups:

- Heuristic algorithms are broad problem-solving strategies that employ a trial-and-error approach rather than an exact answer to obtain an acceptable solution. These algorithms generally scan a vast search space for a suitable solution in an acceptable period of time. Heuristic algorithms cannot guarantee optimality, but they can produce an acceptable answer in a fair period of time. Simulated annealing, genetic algorithms, and particle swarm optimization are all examples of heuristic algorithms.

- On the other hand, gradient-based algorithms use mathematical techniques to find the minimum or maximum of a function. These methods are founded on the idea that a function's gradient leads in the direction of the steepest increase or fall, and that by following this direction, the algorithm can converge to a local minimum or maximum. Gradient-based algorithms can offer accurate solutions, but they are computationally expensive, particularly when the search space is wide, or the function is complex.

The selection of both topology optimization and gradient-based algorithms for this research is based on the recognition that the complexity of the cooling system requires a comprehensive approach that can accommodate multiple design parameters while ensuring the optimization of the cooling system's performance, efficiency, and reliability.

2.2. Gradient-based optimization and the Adjoint method

To initiate the continuous adjoint formulation for topology optimization problems, the derivative of the objective function (known as sensitivity, *G*) with respect to the design variables must be computed in such a way that it is independent of the number of design variables. The sensitivity required for a gradient-based optimization is:

$$G = \frac{\delta J}{\delta b} \cong \frac{J(b + \Delta b) - J(b)}{\Delta b} \tag{3}$$

However, as can be seen in Equation 3, sensitivity (*G*) is directly dependent on the number of design variables, so that it would be necessary to perform such a calculation for each of the design variables, which would imply a very high computational cost if the number of parameters is high. The use of Lagrange multipliers in the derivation of continuous adjoint equations is employed to ensure that the sensitivity is not dependent on the number of design variables [9]. This approach incorporates the constraints of the problem and enables the optimization algorithm to update the Lagrange multipliers and the design variables in a way that satisfies the constraints and improves the objective function.

The primary aim of this study is to introduce a methodology for multi-objective topology optimization of a coupled system involving heat transfer and fluid flow. The focus is on

controlling the recovered thermal power generated over the boundaries from single or multiple heat sources. However, these problems are subject to a set of physical constraints represented by *R*, which can be enforced using a Lagrange function *L*, which is computed according to Equation 4, in which *V* is the domain and is the vector of Lagrangian multipliers that for the adjoint approach will represent the adjoint variables, which are the adjoint pressure (q), adjoint velocity (v) and the adjoint temperature (T_a) as shown in Equation 4.

$$L = J + \int_V \lambda \cdot R \, dV \qquad \lambda = (q\,, v\,, T_a) \tag{4}$$

In this manner, the optimization problem that follows involves computing the sensitivity of the augmented cost function *L* in relation to the design variables *b*:

$$\frac{\delta L}{\delta b} = \frac{\delta J}{\delta b} + \frac{\delta}{\delta b}\int_V \lambda \cdot R \, dV \tag{5}$$

Applying now Leibniz's theorem to expand the derivative term of the integral, leaves Equation 6.

$$\frac{\delta L}{\delta b} = \frac{\delta J}{\delta b} + \int_V \frac{\partial \lambda}{\partial b} \cdot R \, dV + \int_V \lambda \cdot \frac{\partial R}{\partial b} \, dV + \int_S (\lambda \cdot R) \, \frac{\delta x}{\delta b} \, n \, dS \tag{6}$$

If to the latter Equation 6 one applies the fixed-boundary hypothesis (valid for TO) which assumes that the state variables have fixed values at the boundaries of the domain, Equation 7 is obtained. This assumption allows for the elimination of certain terms in the adjoint equations, which reduces the computational cost of solving the adjoint problem.

$$\frac{\delta L}{\delta b} = \frac{\delta J}{\delta b} + \int_V \lambda \cdot \frac{\partial R}{\partial b} \, dV \tag{7}$$

At this stage, what needs to be done is to expand the constraint term *R* which, as we have seen in Equation 2, represents the main equations of conservation of mass (R^p), momentum (R^u) but now with the addition of the energy equation (R^T) due to the existence of heat transfer. Meaning that the solution of the state equations is actually a constraint for the problem [10].

$$R = \{ R^p,\, R^u,\, R^T \} = 0 \tag{8}$$

- <u>Mass conservation:</u>

$$R^p \equiv \nabla \cdot u \tag{9}$$

- <u>Momentum balance:</u>

$$R^u \equiv \nabla \cdot (uu) + \nabla p - \nabla \cdot (\nu \nabla u) + \alpha(\eta) u \tag{10}$$

In Equation 10, it can be observed how the term *"α(η)u"* has been added, which is known as the Brinkman penalization term, where α is the porosity which is updated using the pseudo density (η) as design variable. The Brinkman penalization term is added to the Navier-Stokes equation as a source term, which penalizes the fluid velocity in the porous regions [13].

Porosity (α) refers to the fraction of the total volume of a material or medium that is composed of voids, pores, or empty spaces. In other words, it is the percentage of the total volume of a material that is not occupied by solid material but rather is made up of empty space or voids. Therefore, if the porosity tends to zero, the momentum balance for the fluid is recovered, if on the contrary the porosity tends to infinity it means that the velocity tends

to zero and therefore the transport of temperature in the control volume is dominated by solid diffusion.

- Energy balance:

$$R^T \equiv \nabla \cdot (uT) - \nabla \cdot (D(\eta)\nabla T) \tag{11}$$

As alterations are made to the design variable, the governing equations cause modifications in the flow field. Consequently, the total variation of L encompasses not only changes in the design variable but also adjustments in the primary flow variables such as velocity, pressure, and temperature. For this reason, it is necessary to rewrite Equation 7 by expanding the term $\frac{\partial R}{\partial b}$ as a function of $\frac{\partial u}{\partial b}, \frac{\partial p}{\partial b}, \frac{\partial T}{\partial b}$ (see Equation 12).

$$\frac{\delta L}{\delta b} = \frac{\delta J}{\delta b} + \int_V q \cdot \frac{\partial R^p}{\partial b}\, dV + \int_V v \cdot \frac{\partial R^u}{\partial b}\, dV + \int_V T_a \cdot \frac{\partial R^T}{\partial b}\, dV = \tag{12}$$

$$= \int_V R^q \frac{\partial p}{\partial b} dV + \int_V R^v \frac{\partial u}{\partial b} dV + \int_V R^{T_a} \frac{\partial T}{\partial b} dV + BC^p + BC^u + BC^T + \int_V uv \frac{\partial \alpha}{\partial b} dV + \int_V \frac{\partial D}{\partial b} \nabla \mathrm{T}_a \nabla \mathrm{T} dV$$

being:

$$R^a \equiv \{ R^q, R^v, R^{T_a} \} \tag{13}$$

the set of the adjoint equations:

$$R^q \equiv \nabla \cdot v + \left.\frac{\partial J}{\partial p}\right|_V \tag{14}$$

$$R^v \equiv -\nabla \cdot u - (\nabla v)u - \nabla \cdot \big(2\nu\varepsilon(v)\big) + \alpha v + \nabla q - T\nabla T_a + \left.\frac{\partial J}{\partial u}\right|_V \tag{15}$$

$$R^{T_a} \equiv -\nabla \cdot (uT_a) - \nabla \cdot (D\,\nabla T_a) + \left.\frac{\partial J}{\partial T}\right|_V \tag{16}$$

Notably, the final two components of Equation 12 do not incorporate any state variable derivatives with regards to the design variables. It's crucial to highlight that in cases where the function J is designated at the boundary S and has a zero value in the internal domain:

$$\left.\frac{\partial J}{\partial p}\right|_V = 0\,;\ \left.\frac{\partial J}{\partial u}\right|_V = 0\,;\ \left.\frac{\partial J}{\partial T}\right|_V = 0 \tag{17}$$

According to the conditions of Equation 17, the terms $\frac{\partial J}{\partial p}, \frac{\partial J}{\partial u}, \frac{\partial J}{\partial T}$ in Equations 14, 15 and 16 disappear. The adjoint equations within the internal domain are, as a result, not reliant on the cost function of the problem. However, it's worth noting that this assertion doesn't hold true for the boundaries, and utilizing distinct cost functions necessitates the implementation of dissimilar boundary conditions for the identical solver. In essence, the applicability of different boundary conditions stems from the fact that the behaviour of the cost function at the boundaries can significantly influence the solutions obtained from the solver. Therefore, to obtain accurate and reliable results, it's crucial to carefully select and apply the appropriate boundary conditions that correspond to the cost function being utilized.

2.3. Topology Optimization using Continuous Adjoint

Subsequently, Equation 12 must be implemented within the adjoint CFD solver. The optimization problem is downgraded to minimize the augmented objective function *L*, which has been shown to be a function of velocity, pressure, temperature, and the pseudo density η (used as a control variable).

This work employs a topology optimization strategy where solid material is introduced into the fluid domain via a density-based method. The goal is to obtain a pseudo density field with values ranging from 0 (solid) to 1 (fluid). A pseudo density value of 1, results in the recovery of governing equations for the fluid, while a value of 0 leads to zero flow velocity and solid diffusion dominating temperature transport within the control volume. However, this approach can result in ill-posed problems, and to address this issue, a penalty is introduced to convert the discrete pseudo density into a continuous variable, resulting in a binary solution. The pseudo-density is also used in the determination of material properties, such as density, specific heat, thermal flow diffusivity, and porosity, which are computed using the Rational Approximation of Material Properties (RAMP) model.

When dealing with thermal cooling for power electronics in propulsion systems, it is essential to restrict the overall pressure drop within the cooling circuit while effectively eliminating heat. To achieve this objective, the cost function *J* is formulated as follows:

$$J = w_1 J_1 + w_2 J_2 \tag{18}$$

Where J_1 is the mechanical power dissipated by the fluid through the boundaries, while J_2 is the net thermal power recoverable from the domain.

$$J_1 = -\int_S \left(p + \frac{1}{2}u^2\right) u \cdot n \, dS \tag{19}$$

$$J_2 = \int_S (\rho C_p T) u \cdot n \, dS \tag{20}$$

The goal is to maximize J_2 (the recoverable thermal power) while minimizing J_1 (the mechanical power dissipated by the fluid). However, since J_1 and J_2 have different magnitudes and are related to different features of the system (flow field for J_1 and temperature transport and diffusion for J_2), they need to be normalized to be compared.

One possible normalization approach is to compute the optimal values of J_1 and J_2 respectively from the optimization of the fluid problem and the thermal problem. These values can then be used to scale the corresponding objective functions. Finally, the weighted sum method is applied to perform the multi-objective optimization, where the weights determine the importance of each objective function in the overall optimization.

$$J = w\overline{J_1} - (1 - w)\overline{J_2} \tag{21}$$

In Equation 21, $\overline{J_1}$ and $\overline{J_2}$ are the normalized functions and $w \in (0,1)$ the weighting factor. The weighting factor is a parameter used to assign different levels of importance or significance to different components or objectives within the optimization problem. For this particular case, it is used to control the balance between thermal performance and mechanical power dissipation. A higher weighting factor would prioritize minimizing the mechanical losses while a low value of *w* gives higher importance to maximize heat transfer capabilities. In this research, the weighting factor will be varied to assess its impact on fluid flow characteristics in the context of a cooling system optimization.

Once the objective function is defined, the process of applying optimization constraints starts. This results in a constrained optimization problem, where the constraints are the governing or state equations. To solve this optimization problem, the following constraints must be respected:

- The first constraint is to limit the maximum amount of material that can be added to the system being optimized. This constraint is essential to prevent the optimization from resulting in trivial solutions where the entire system becomes solid. Such solutions are not practically useful and may lead to unphysical results. Therefore, the maximum quantity of material to be added to the domain must be set in a manner that ensures the solution space is not trivial, while still allowing for meaningful and feasible solutions.

- The second constraint involves the governing equations that describe the behaviour of the system being optimized. These equations must be enforced as constraints using the Lagrange multipliers method, which involves introducing additional variables into the optimization problem. This constraint ensures that the solutions obtained are physically meaningful and satisfy the governing equations.

2.4. Boundary Conditions for the Adjoint Problem

Boundary conditions are essential in the adjoint optimization method as they play a crucial role in determining the optimal solution for the cooling system. In the context of the adjoint method for optimizing cooling systems, boundary conditions refer to the set of constraints that must be satisfied by the cooling system. These constraints can be physical, such as the temperature and pressure requirements of the cooling system, or design-related, such as the size and shape of the cooling channels. Therefore, to successfully complete the solution of the adjoint equations, boundary conditions are needed for each of the balance equations:

$$BC^a \equiv \{\, BC^p, BC^v, BC^T \,\} \tag{22}$$

Their general form is expressed in Equations 23-25. The specific formulation of the adjoint boundary conditions depends on the kind of boundary conditions applied to the flow variables in the primal problem. For the cases considered in this paper, these aspects will be discussed throughout this section.

$$BC^p = \int_S \left(v \cdot n + \frac{\partial J}{\partial p}\right)\frac{\partial p}{\partial b}\, dS \tag{23}$$

$$BC^u = \int_S (n \cdot (u \cdot v) + v(u \cdot n) + v(n \cdot \nabla)v - qn - \frac{\partial J}{\partial u} + T_a T n)\frac{\partial u}{\partial b}\, dS - \int_S v(n \cdot \nabla)\frac{\partial u}{\partial b} v\, dS \tag{24}$$

$$BC^T = \int_S \left(n \cdot u\, T_a + Dn \cdot \nabla T_a + \frac{\partial J}{\partial T}\right)\frac{\partial T}{\partial b}\, dS - \int_S (T_a\, Dn) \cdot \nabla\left(\frac{\partial T}{\partial b}\right) dS \tag{25}$$

The adjoint variables q and v are not determined but its value is chosen in such a way that the condition $\boldsymbol{BC^a = 0}$ is enforced, since in this way everything is significantly simplified.

- Inlet:

For the inlet, a common boundary condition for incompressible flows has been used to define the velocity ($\boldsymbol{u}$) and temperature ($\boldsymbol{T}$) at the inlet, so that Equations 23-25 are simplified as follows:

$$BC^p = \int_S \left(v \cdot n + \frac{\partial J}{\partial p}\right)\frac{\partial p}{\partial b}\, dS \tag{26}$$

$$BC^u = -\int_S \nu(n\cdot\nabla)\frac{\partial u}{\partial b} v\, dS \tag{27}$$

$$BC^T = -\int_S (T_a\, Dn)\cdot\nabla\left(\frac{\partial T}{\partial b}\right) dS \tag{28}$$

The relations for the boundary conditions can be further manipulated to obtain the following relations (being v_t and v_n the tangential and normal components of the adjoint velocity):

$$v_t = 0 \tag{29}$$

$$v_n = -\frac{\partial J}{\partial p} \tag{30}$$

$$(n\cdot\nabla)q = 0 \tag{31}$$

$$T_a = 0 \tag{32}$$

- Outlet:

At the outlet, zero Neumann conditions are imposed for the velocity and the temperature, while the value of the pressure is fixed (hence being $\partial p/\partial\,\eta = 0$). A zero Neumann condition at the outlet is a boundary condition that specifies that there is no net mass or energy flow across the boundary.

$$BC^u = \int_S (n\cdot(u\cdot v) + v(u\cdot n) + \nu(n\cdot\nabla)v - qn - \frac{\partial J}{\partial u} + T_a Tn)\frac{\partial u}{\partial b}\, dS \tag{33}$$

$$BC^T = \int_S \left(n\cdot u\, T_a + Dn\cdot\nabla T_a + \frac{\partial J}{\partial T}\right)\frac{\partial T}{\partial b}\, dS \tag{34}$$

The boundary conditions for q, the tangential component of the adjoint velocity v_t, and for T_a can be directly extracted:

$$q = u\cdot v + u_n v_n + \nu(n\cdot\nabla)v_n + \frac{\partial J}{\partial u_n} + T_a T \tag{35}$$

$$u_n v_t + \nu(n\cdot\nabla)v_t = -\frac{\partial J}{\partial u_t} \tag{36}$$

$$u_n T_a + Dn\cdot\nabla T_a = -\frac{\partial J}{\partial T} \tag{37}$$

The boundary conditions for the normal component of the adjoint velocity v_n are obtained from continuity equation (being $\nabla_{||}$ the in-plane component of the derivatives at the boundary):

$$(n\cdot\nabla)v_n = \nabla\cdot v - \nabla_{||}\cdot v_t = -\nabla_{||}\cdot v_t \tag{38}$$

- Adiabatic wall

The boundary conditions for pressure and velocity are the same as at the inlet boundary (Neumann for pressure and Dirichlet for velocity). This results in the boundary conditions for adjoint pressure and velocity being expressed in Equations 29-31. The normal derivative of temperature is fixed, and velocity is equal to zero, leading to the boundary condition for adjoint temperature being defined as follows:

$$Dn\cdot\nabla T_a = -\frac{\partial J}{\partial T} \tag{39}$$

- Fixed temperature wall

If the temperature is fixed at the wall, then the derivation of the boundary condition for T_a leads to $T_a = 0$. The boundary conditions for the adjoint pressure and velocity are the ones expressed in Equations 29-31.

3. Solver implementation

In this section, the implementation of the adjoint optimization method for the cooling system of an electrical propulsion engine in an aircraft using the OpenFOAM numerical solver is explained and presented. The implementation is divided into two parts: the solution of the primal flow based on the SIMPLE method, and the solution of the adjoint problem by using the adjoint equations previously derived from the cost function.

3.1. Solution of the primal flow

The process is based on the SIMPLE method (Semi-Implicit Method for Pressure-Linked Equations), which is a well-established algorithm for solving fluid flow problems numerically, based on the concept of pressure-velocity coupling. All the fundamentals of the SIMPLE method will be explained including all the flux of equations, and how it is used to solve the primal flow of the cooling system.

First, the flow variables, such as velocity and pressure, are initialized to some initial values which serve as a starting point for the iterative process. Next, the momentum equations, which describe the motion of fluid flow, are solved using the current values of the flow variables. This results in an intermediate velocity field (u^*) which does not satisfy continuity equation, that's why then the pressure correction equation (Poisson's equation) is then derived from the continuity equation and used to correct the pressure field. Then, the new pressure is used to correct the velocity field. Finally, the transport of temperature equation is added to get the temperature distribution in an incompressible solver without the need of adding the energy equation. These steps are repeated until the solution converges to a steady state. The iterative process continues until the change in the flow variables between successive iterations is below a certain tolerance value. This iterative process is graphically illustrated in the flowchart in Figure 1.

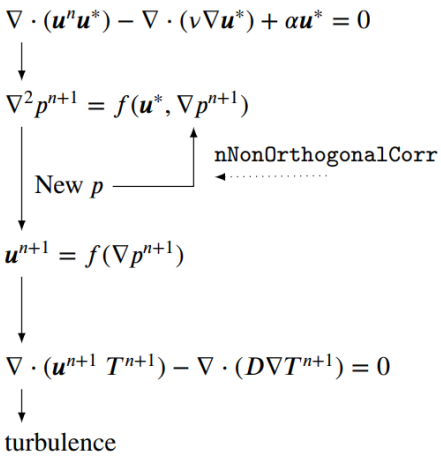

Figure 1: Flow chart of the solution method for the primal flow [1].

Once the schematic flow shown in Figure 1 is clear, a detailed description of each of the equations involved in each iteration of the solver is given. The momentum predictor equation is the one shown in Figure 1, however, the pressure equation or also called Helmholtz equation for compressible flows and Poisson equation for incompressible flows (see Equation 40), is a combination of the mass and momentum conservation equations.

$$\nabla^2 p^{n+1} = \frac{1}{\Delta t}[\nabla \cdot (\rho\, u^*)] \tag{40}$$

An important fact to consider with the Poisson equation is the fact that it includes a Laplacian, which is highly affected by the non-orthogonality of the mesh, and which is necessary to correct with the non-orthogonal correctors, however in this particular case a totally orthogonal mesh is used, so the non-orthogonal correctors are not necessary.

Once we have the pressure field, the intermediate velocity field has to be corrected. The velocity correction is achieved by subtracting the gradient of the pressure correction term from the intermediate velocity field. This ensures that the final velocity field satisfies both the momentum and continuity equations. It is important to note that the velocity correction step is an iterative process. It is needed to repeat the velocity correction sub-step until the velocity field converges to a steady state.

On the other hand, during and through all these iterative processes, dampers are needed on certain variables such as pressure, which is why under-relaxation factors are used. They are crucial to limit the change of the values of the main flow variables from outer iteration to outer iteration in order to avoid instabilities especially in the first outer iterations. To explain how it works, we first consider the discretised algebraic equation for a general variable ϕ and at a certain iteration n (see Equation 41). In this equation, A_P represents the main diagonal matrix elements, A_l the remaining parameters of the main matrix and Q_P the source vectors components.

$$A_P \cdot \phi_P^n + \sum_l A_l \cdot \phi_l^n = Q_P \tag{41}$$

The under-relaxation factors are defined in Equation 42, which shows how the value of the variable ϕ_P^n is constrained by α_ϕ to take values between its value from the previous iteration ϕ_P^{n-1} and the value from the transport equation ϕ_P^{new}.

$$\phi_P^n = \phi_P^{n-1} + \alpha_\phi \cdot (\phi_P^{new} - \phi_P^{n-1}) \tag{42}$$

The under-relaxation factor takes values between 0 and 1, so that if it takes the value of 0, the new value of the variable ϕ_P^n takes the value equivalent to that of the previous iteration ϕ_P^{n-1}, and if it takes the value of 1, ϕ_P^n takes the direct value of that calculated in the transport equation ϕ_P^{new}. The under-relaxation factors increase the convergence of the solution by increasing numerically the diagonal dominance of the main matrix and their values taken depend on each case, however, a clever way to apply them is to assign small values of alpha α_ϕ in the early outer iterations and increase their value until reaching 1 when the solution approaches convergence.

3.2. Solution of the adjoint problem

The procedure to solve the adjoint problem is quite similar to the one applied for the primal flow but working with the adjoint variables and equations. One of the main features is the fact that the adjoint temperature T_a can be calculated completely independent of the adjoint pressure q and velocity v, so for convenience it is the first thing to be calculated.

To calculate it, the transport equation for temperature is used, also consisting of both the convective and diffusive terms. Then, as in the primal flow, once the adjoint temperature is known, we proceed to predict the adjoint velocity field ($\boldsymbol{v}^*$) but ignoring the adjoint pressure gradient

since later this velocity field will be corrected with the pressure equation to comply with mass conservation, basically the same as in the primal flow (see Figure 2). The rest of the steps are analogous to the primal flow but dealing with the adjoint variables. In contrast to its primal counterparts, the adjoint momentum balance exhibits linearity. However, several numerical challenges arise due to various factors. One such factor is the term "∇uv", also known as Adjoint Transpose Convection (ATC), which acts as an instability source for the adjoint equation solution [8].

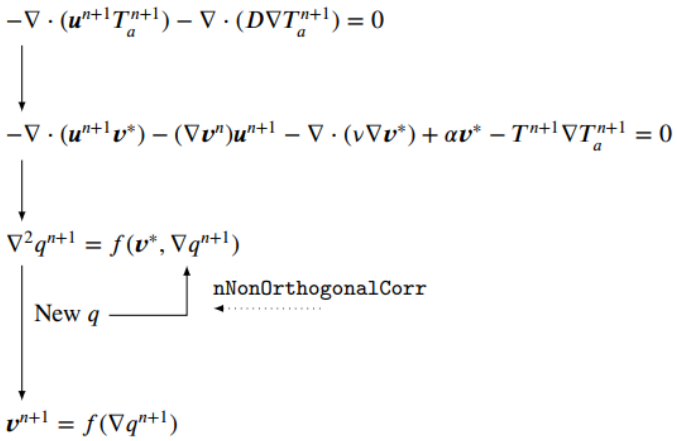

Figure 2: Flow chart of the solution method for the adjoint problem [1].

4. Set-up and post-processing

This thesis aims to evaluate the optimization of a cooling system for an aircraft using adjoint optimization techniques. The simulations have already been conducted in OpenFOAM, and the purpose of this section is to provide a commentary on the obtained results.

The evaluation will be performed on the same setup and geometry for different weighting factors (w), which range from 0.1 to 0.8. As previously seen, the cost function used for this evaluation is composed of two terms, the first of which represents the mechanical power dissipated by the fluid through the boundaries, while the second term represents the net thermal power recoverable from the domain. The weighting factor plays a crucial role in determining the optimal solution. The importance of each term in the cost function can be maximized or minimized by adjusting the weighting factor, which determines the relative importance of each term. The ideal value of the weighting factor will depend on the specific requirements of the cooling system.

Additionally, the evaluation of the system with a lower thermal diffusivity will be performed. Thermal diffusivity is a material property that affects the heat transfer characteristics of the system. Lowering the thermal diffusivity will enable the evaluation and better understanding of the system's performance under different thermal conditions.

The parameters under investigation include the weighting factor in the optimization algorithm, the thermal diffusivity of the solid material, the k coefficient in the RAMP interpolation method, and the amplitude of the filter used for data smoothing. By studying these parameters individually, their impact on the cooling system's performance, including flow characteristics, heat transfer efficiency, and the balance between mechanical and thermal aspects, will be assessed. The insights gained from this research will contribute to the optimization and design of more efficient cooling systems. But will first briefly describe both the geometry, the mesh and the boundary conditions.

4.1. Geometry, mesh and boundary conditions

The geometry of a simulation is a fundamental aspect that plays a crucial role in accurately capturing the physical behaviour of the system under consideration. In this section, the geometry of an OpenFOAM simulation will be explored. This simulation involves a 2D cavity flow problem, where fluid is driven through a square cavity with adiabatic and hot walls. The simulation is modelled using the Navier-Stokes equations, and it is carried out using the OpenFOAM software package. A detailed description of the geometry used in this simulation, including the grid generation process, boundary conditions, and any simplifying assumptions made to model the physical system, will be provided in this section.

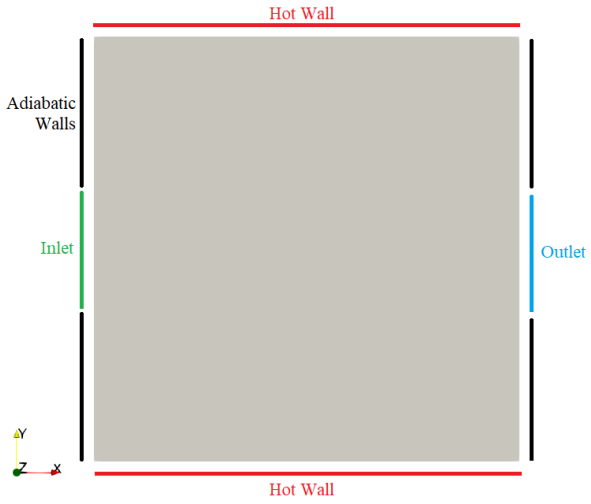

Figure 3: Geometry scheme.

The geometry is presented in Figure 3, which shows different sections corresponding to the different boundaries. It can be seen that it is a square cavity in which the inlet and outlet are facing each other with adiabatic walls around them. When the fluid enters the inlet and travels along the cavity to the outlet, it will experience temperature and density gradients due to the presence of two hot walls located at the top and bottom of the cavity.

Hereafter, the mesh generation process is an essential step in any computational fluid dynamics (CFD) simulation. In this simulation, an orthogonal mesh (see Figure 4) is generated using the blockMesh command in OpenFOAM and it has cell size equal to 0.001m. This type of mesh can reduce errors and numerical artifacts that may arise due to skewed cells or distorted meshes which would strongly affect the Laplacians and the reliability of the results.

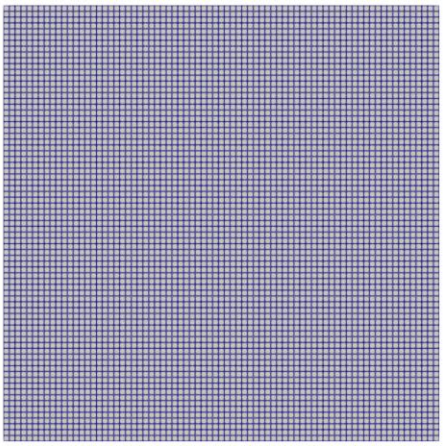

Figure 4: Mesh.

To accurately model the physical system, boundary conditions are assigned to the different walls of the cavity and are all presented in Table 1. It is important to note the fact that a dimensionless temperature is taken, according to the Equation 43. So, a value of 0 means that the temperature is equal to the T_{in} and a value of 1 means that the temperature is equal to the temperature of the hot wall.

$$\frac{T - T_{in}}{T_w - T_{in}} \tag{42}$$

Patches	Velocity	Adjoint Velocity	Pressure	Adjoint Pressure	Temperature	Adjoint Temperature	Sensitivity
Inlet	*Calculated*	0**	Zero gradient	Zero gradient	0	0*	Zero gradient
Outlet	0	0**	0	0**	Zero gradient	0**	Zero gradient
Hot Walls	0	0	Zero gradient	Zero gradient	1	0	Zero gradient
Adiabatic Walls	0	0	Zero gradient	Zero gradient	Zero gradient	Zero gradient	Zero gradient
Front and Back	-	-	-	-	-	-	-

Table 1: Boundary conditions set-up.

There are several things to note from those shown in Table 1, the first of which is to clarify the super indexes found in some of the values. Those with "*" mean that they have a zero gradient boundary condition with a uniform value assigned, i.e., this boundary condition sets the parameter values at the corresponding patch to a certain value and assumes that the derivative of the field normal to the boundary is zero. On the other hand, the super index "**" appears, which means that it is of the adjoint type (it is a specialized boundary condition that is used in adjoint optimization problems, where the field of the corresponding variable is part of the objective function or the optimization constraints) and it has a uniform value assigned to it.

Finally, the boundary condition of the velocity (*U*) at the inlet is calculated by a function which obtains the velocity values at the inlet using the log-law boundary layer theory and assigns them to the velocity field at the boundary. This results in a parabolic velocity profile that satisfies the boundary conditions of the problem.

4.2. Results

The following section presents the results of the simulations conducted to optimize the topological form of a cooling system modelled as a 2D cavity. The objective was to investigate the influence of different weighting factors on the optimal cavity design for two cases: one with a given thermal diffusivity ($D = 9.75 \cdot 10^{-5}\, m^2 s^{-1}$) and another with lower thermal diffusivity ($D = 2.1 \cdot 10^{-6}\, m^2 s^{-1}$). Additionally, a parametric analysis was performed to examine the effects of varying the coefficient *k* (RAMP interpolation method) and the amplitude of the filter used on the simulation results.

The optimization process aimed to find the optimal flow pattern inside the cavity by adjusting the topology. It is crucial to bear in mind that there are still two main objectives behind each optimisation: maximizing the recoverable thermal power and minimizing the mechanical power dissipated.

4.2.1. Solid 1 ($D = 9.75 \cdot 10^{-5}\ m^2 s^{-1}$)

By analysing the first outcomes (see Figure 5), we can gain insights into how the flow behaviour inside the cavity changes as the importance shifts between maximizing recoverable thermal power and minimizing mechanical dissipation. Specifically, the focus is on understanding how the flow is redirected to the hot walls or streamlined towards the outlet based on the selected weighting factor. With low weighting factors, the priority is given to maximizing recoverable thermal power that's why the optimization process focuses on redirecting the flow towards the hot walls to enhance convective heat transfer by adding solid at the centre of the cavity. The increased contact area between the fluid and the hot walls facilitates efficient heat absorption, thereby maximizing the recoverable thermal power.

On the other hand, as the weighting factor is increased, the simulations demonstrate that the optimization process aims to streamline the flow path, minimizing deviations and promoting a direct path from the inlet to the outlet. The motivation behind this behaviour lies in the optimization process's objective to reduce energy losses associated with fluid flow. By minimizing deviations and flow resistance, the optimization process effectively decreases pressure drop, turbulence, and other factors contributing to energy dissipation.

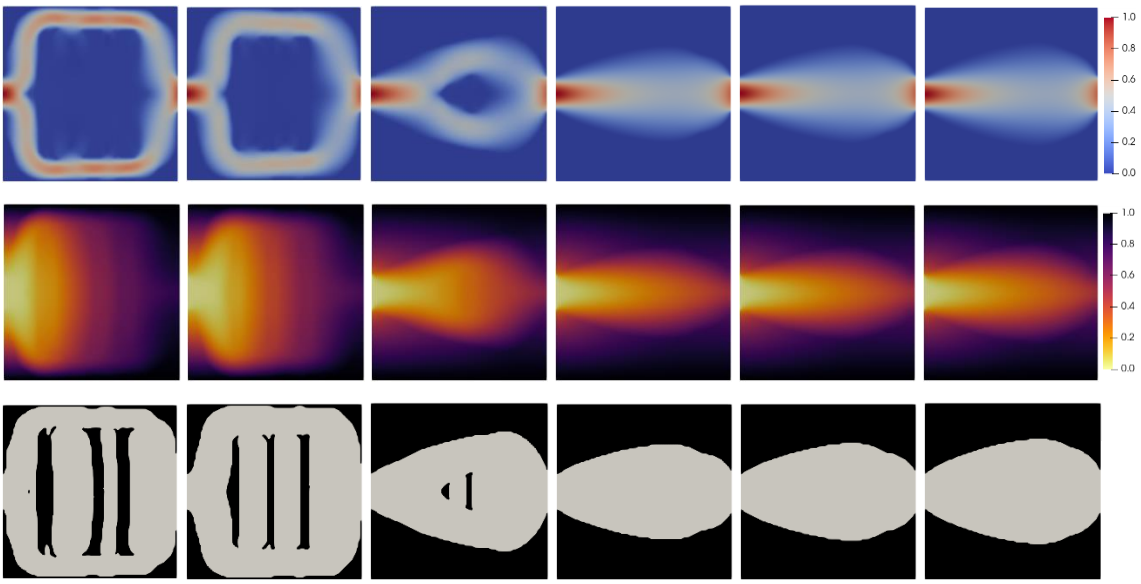

$w = 0.1$ $w = 0.3$ $w = 0.5$ $w = 0.6$ $w = 0.65$ $w = 0.8$

Figure 5: Normalized velocity (U/max (U)), temperature contour plots and topology of the cavity corresponding to different weighting factors.

Bear in mind that all the results are optimal results for each of the weighting factor, however, selecting the optimum weighting factor in the context of the simulations involves finding a balance between maximizing the recoverable thermal power and minimizing the mechanical power dissipated. A notable feature of the results is that from $w = 0.6$ onwards, neither the topology nor the main flow properties change significantly, which is something that will be discussed in the pareto chart analysis later on.

4.2.2. Solid 2 ($D = 2.1 \cdot 10^{-6}\ m^2 s^{-1}$)

The results of reducing the thermal diffusivity are shown below (see Figure 6). What can be observed in this case is that the optimization process may still focus on redirecting the flow towards the hot walls to enhance convective heat transfer for low weighting factors but in a very different way. However, the presence of a solid material with significantly lower thermal diffusivity can hinder heat conduction and reduce the efficiency of heat transfer from the solid to the fluid. Lower thermal diffusivity implies that heat is conducted more slowly through the solid material. This is why it is no longer of interest to add material to the hot walls so that the fluid is

directly in contact with the hot walls and not with the solid. In addition, it is observed that the flow deviates sharply for a weighting factor of 0.65 and even more, which is quite different from the other case (in which the flow was already streamlined for $w = 0.5 - 0.6$).

In the case where the solid has high thermal diffusivity (for high weighting factors), the addition of material forming a pipe-like structure that streamlines the flow from the inlet to the outlet is a result of the optimization process aiming to minimize mechanical dissipated power (see Figure 5). However, when the thermal diffusivity of the solid is reduced, the optimization process yields a different result. Instead of adding material to streamline the flow, only a small diverging nozzle is formed at the inlet, and the rest of the cavity remains empty without any additional material. This behaviour suggests that, for the given conditions, the optimization process does not find it beneficial to add material to redirect the flow or further streamline it. The reason behind this difference could be attributed to the reduced thermal diffusivity's influence on the heat transfer dynamics within the system. Lower thermal diffusivity implies slower heat conduction, which can lead to the formation of localized high-temperature regions near the hot walls. In such cases, the optimization process may find it more effective to allow the flow to naturally distribute and dissipate heat rather than adding material to further manipulate the flow pattern.

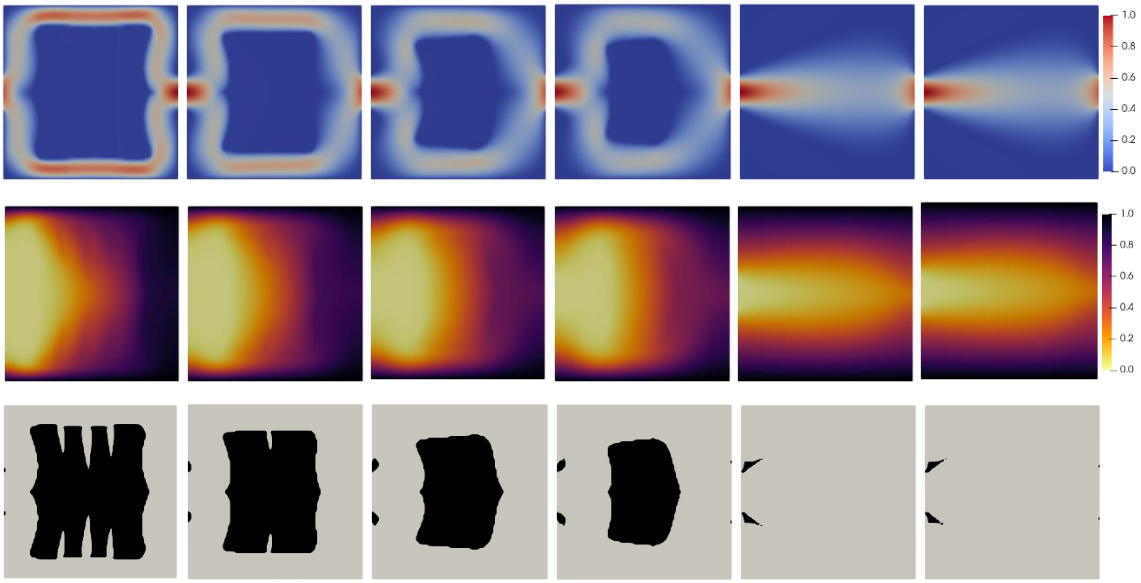

Figure 6: Normalized velocity ($U/max\ (U)$), temperature contour plots and topology for different weighting factors with a different thermal diffusivity ($D = 2.1 \cdot 10^{-6}\ m^2 s^{-1}$).

4.2.3. Pareto front analysis

In order to assess the trade-off between mechanical power dissipation and recoverable thermal power in the cooling system, Pareto fronts have been constructed for both the case with higher thermal diffusivity and the case with lower thermal diffusivity. The Pareto fronts provide a graphical representation of the optimal solutions that balance these two objectives. Comparing the Pareto fronts for the two different thermal diffusivities provides valuable insights into how the thermal properties of the solid affect the trade-off between mechanical power dissipation and recoverable thermal power. It allows for a comparative analysis of the performance and optimization potential of the cooling system under different thermal diffusivity conditions.

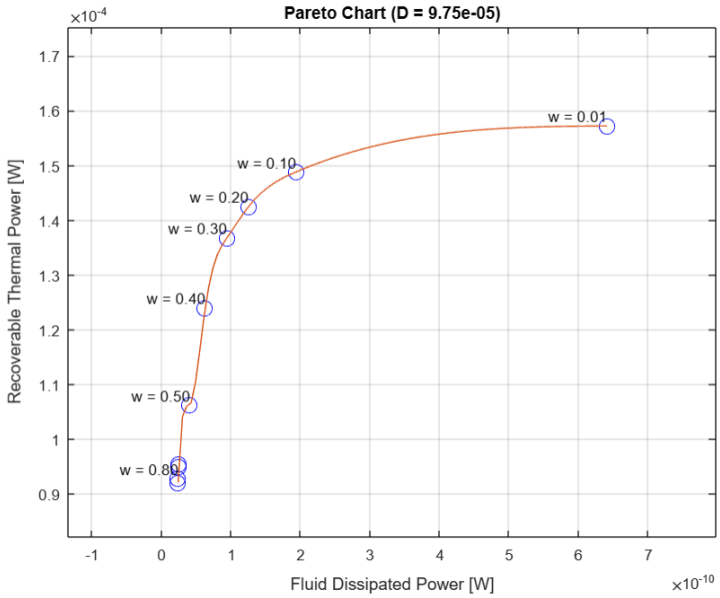

Figure 7: Pareto front for $D = 9.75 \cdot 10^{-5}\ m^2 s^{-1}$.

The observations made in Figure 7 and 8, where a convex curve is depicted for both cases, highlight certain trends and patterns in the trade-off between fluid dissipated power and recoverable thermal power.

Firstly, in Figure 7 it can be observed that for weighting factors above approximately 0.3, increasing the weighting factor has a limited impact on the fluid dissipated power. This suggests that beyond this point, further prioritizing recoverable thermal power does not lead to significant reductions in fluid dissipation. In other words, the optimization process reaches a point of diminishing returns where increasing the importance given to recoverable thermal power does not result in substantial improvements in reducing fluid dissipated power. On the other hand, the recoverable thermal power is significantly affected as the weighting factor increases. This implies that emphasizing recoverable thermal power leads to substantial gains in harnessing and utilizing the heat energy within the system

In Figure 8, which represents the graph for the solid with reduced thermal diffusivity, some noticeable differences can be observed. The clustering of points and higher values of recoverable thermal power for weighting factors between 0.1 and 0.5 indicate that for this particular solid, there is a more significant impact of the weighting factor on the recoverable thermal power. This suggests that optimizing for recoverable thermal power in the case of reduced thermal diffusivity can lead to more pronounced improvements in capturing and utilizing heat energy.

The overlapping and almost identical results observed for weighting factors of 0.6 and above in both cases may indicate that the optimization process reaches a plateau where further increasing the weighting factor does not result in substantial changes in the trade-off between fluid dissipated power and recoverable thermal power.

Overall, the observations in both Figure 7 and Figure 8 demonstrate the influence of the weighting factor on the trade-off between fluid dissipated power and recoverable thermal power. The results highlight the importance of finding an optimal balance between these objectives and suggest that the impact of the weighting factor can vary depending on the thermal diffusivity of the solid being analyzed.

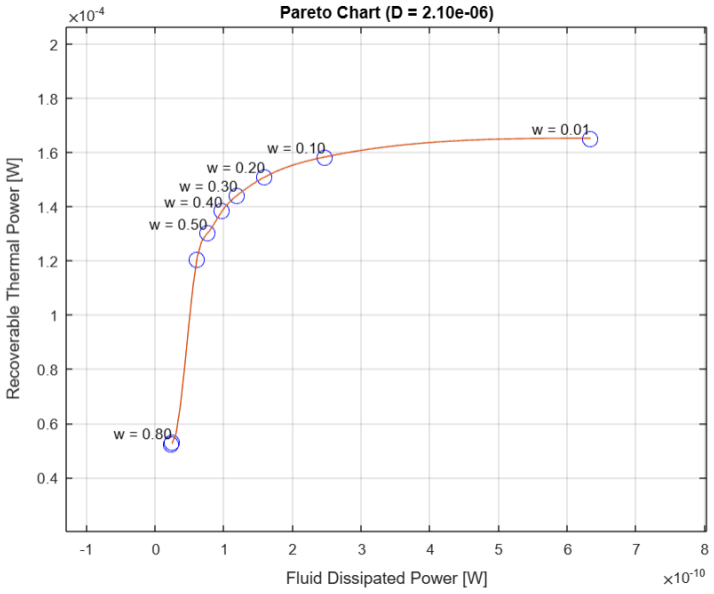

Figure 8: Pareto front for $D = 2.10 \cdot 10^{-6}\ m^2 s^{-1}$.

4.2.4. Sensitivity analysis for the "*k*" coefficient in RAMP method

In the context of the RAMP interpolation method utilized in OpenFOAM, the *k* coefficient plays a crucial role in regulating the steepness of the interpolation function. The RAMP method is employed to smoothly transition between different values within a given range. The RAMP function, in essence, allows for a gradual change from one value to another over a specified interval. This function is particularly useful in situations where a sudden transition would not accurately represent the physical behaviour or desired simulation outcome. By controlling this *k* coefficient, one can adjust the steepness or smoothness of this transitions. The focus of this analysis is to investigate the impact of varying the value of *k* in the RAMP interpolation method on the simulation results to quantify the corresponding effects on the cooling system's performance (see Figure 9).

If *k* is less than 1, the RAMP function exhibits a gentler and smoother transition. This lower value of *k* causes the interpolation to be less sensitive to changes in the input data, resulting in a more gradual variation between the values. Consequently, the overall impact of any fluctuations or deviations in the input data is diminished. Conversely, when *k* is greater than 1, the RAMP function becomes steeper and more sensitive to changes in the input data. The higher value of *k* amplifies the variations in the input values, leading to a more pronounced and rapid transition between the given values. Finally, if *k* is set to 1, the RAMP function behaves linearly, resulting in a uniform transition between the given values. In this case, the interpolation is characterized by a balanced change, without any amplification or attenuation of the input data.

However, as can be seen in Figure 8, for values close to zero there is a large impact on the results, but for values higher than 0.4, the impact is null. Nevertheless, when the value of *k* is close to 0 or very small, it results in a highly gentle and gradual transition between the given values, and the RAMP function tends to assign greater weight to the lower boundary value, resulting in a less significant sensitivity to changes in the input data. Anyway, it is noticeable that for low values of *k*, the optimisation process tends to prioritise the thermal recoverable power as more material is added to the centre in order to divert the flow towards the hot walls.

It is important to note that the behaviour of the simulation results can be influenced by various factors beyond just the *k* value. The specific characteristics of the cooling system and the nature of the simulations being performed can contribute to the observed effects.

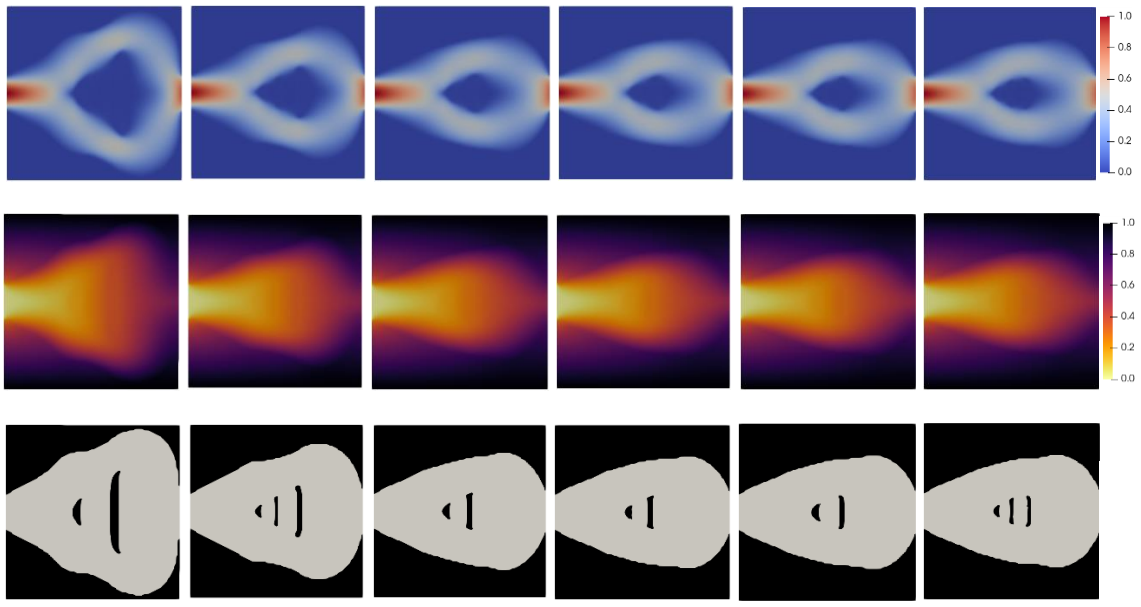

$k = 0.025$ $k = 0.05$ $k = 0.1$ $k = 0.4$ $k = 1$ $k = 2$

Figure 9: Normalized velocity ($U/max\ (U)$), temperature contour plots and topology of the cavity corresponding to $w = 0.5$ and $D = 9.75 \cdot 10^{-5}\ m^2 s^{-1}$ but for different values of k.

Next, the same analysis has been carried out but with the solid with less thermal diffusivity (see Figure 10), and what has been observed is that there are not as significant changes as in the previous case. In this scenario, even when the *k* coefficient is varied across different values, the impact on the simulation results may be practically null. The slower heat conduction restricts the influence of the *k* coefficient in inducing significant changes in the temperature distribution or overall behaviour of the system. The reduced thermal diffusivity acts as a dampening effect, limiting the sensitivity of the simulation results to variations in the "k" coefficient.

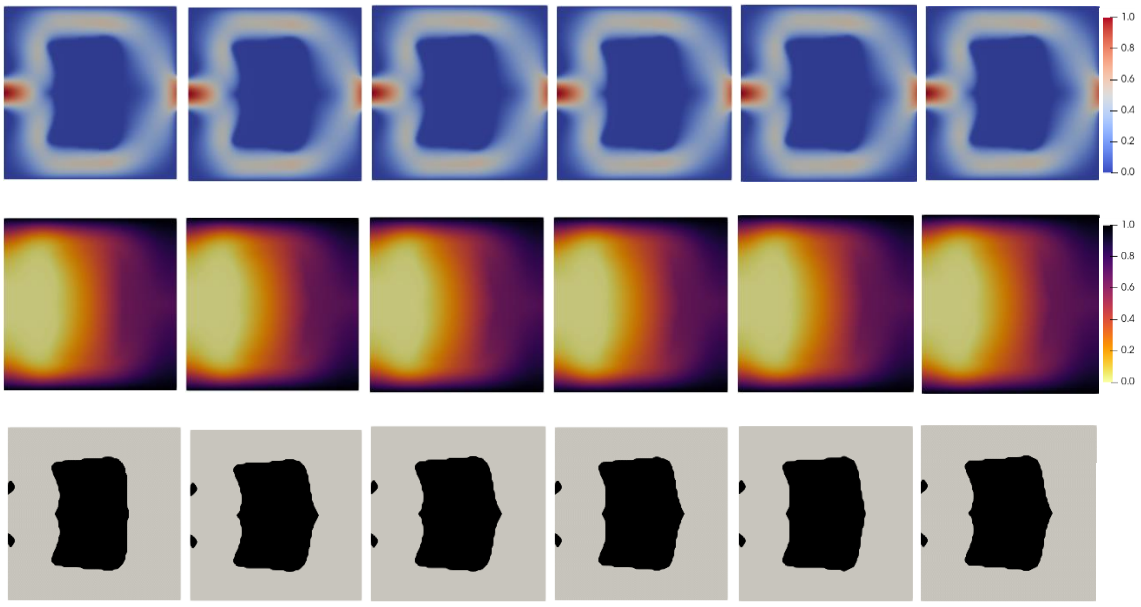

$k = 0.025$ $k = 0.05$ $k = 0.1$ $k = 0.4$ $k = 1$ $k = 2$

Figure 10: Normalized velocity ($U/max\ (U)$), temperature and topology contour plots corresponding to $w = 0.5$ and $D = 2.1 \cdot 10^{-6}\ m^2 s^{-1}$ but for different values of k.

This impact on both recoverable thermal power and mechanical power dissipated can be seen graphically in Figure 11. It can be clearly observed that there is roughly a linear trend in which, as the value of *k* is reduced close to 0, the values of both objective functions increase. On the other hand, by raising the value of *k* even above 1, the value of the objective functions decreases. Moreover, it is noticeable in the first case (a) how reducing the coefficient *k* has more impact than increasing it. Finally, in the case of reducing the thermal diffusivity (b), it is observed that varying the coefficient *k* has practically no impact on the results.

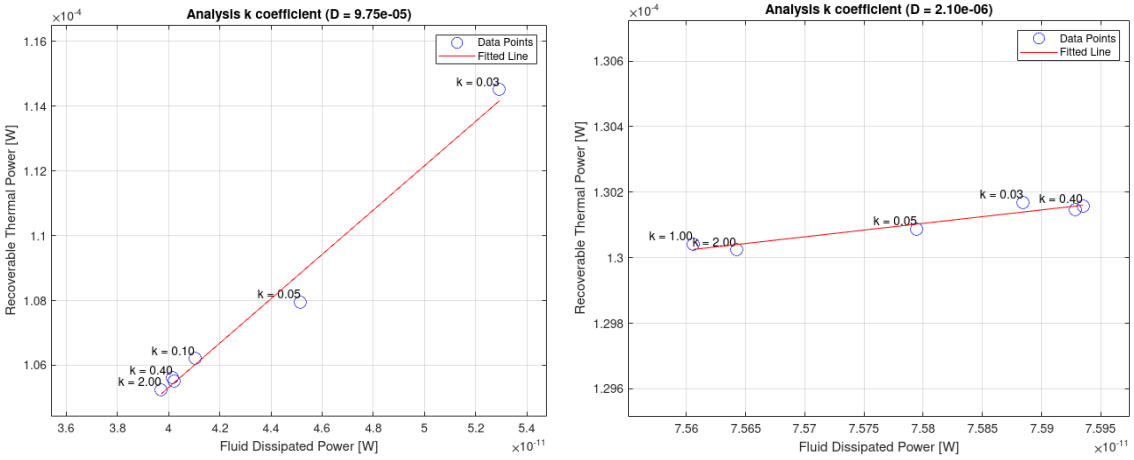

(a) (b)

Figure 11: Evolution of the impact on the recoverable thermal power and mechanical dissipated power for different values of k and different thermal diffusivities: (a) $D = 9.75 \cdot 10^{-5}\ m^2 s^{-1}$ and (b) $D = 2.1 \cdot 10^{-6}\ m^2 s^{-1}$..

This effect is most easily and visually seen in the bar graph shown in Figure 12, where changes of up to almost 30% in dissipated power are observed in case (a). However, it is easy to see that it is not profitable to reduce the value of *k* since it increases the dissipated power (which is something to be minimised) more than the recoverable thermal power. On the other hand, in case (b) the percentage change in the objective functions is practically negligible.

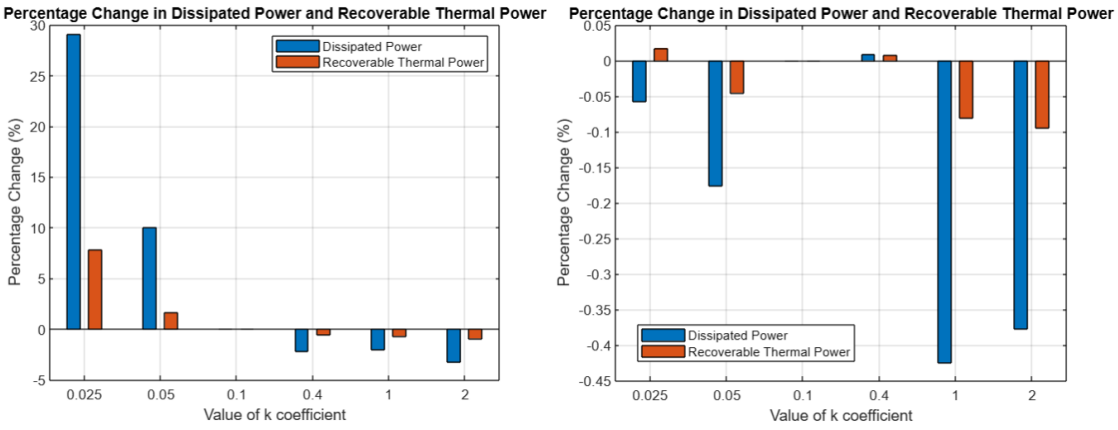

(a) (b)

Figure 12: Bar graph which accounts for the percentage change of both objective functions with respect to the base case ($k = 0.1$) for both thermal diffusivities: (a) $D = 9.75 \cdot 10^{-5}\ m^2 s^{-1}$ and (b) $D = 2.1 \cdot 10^{-6}\ m^2 s^{-1}$.

4.2.5. Sensitivity analysis for the filter width

Smoothing, or filtering, is a common technique used in computational simulations to reduce noise, eliminate small-scale variations, or create a more regular representation of the data. The aim is to explore the impact of adjusting the amplitude of a filter to be around the size of the cell size in a computational simulation. By setting the amplitude of the filter to this specific value, we will investigate how it affects the results and the behaviour of the scalar field being filtered. Different sizes will be evaluated for the amplitude of the filter f, one equal to the mesh cell size ($f = 0.001$), one larger and one smaller.

The purpose of smoothing a scalar field with a filter is often to achieve a more gradual or uniform transition between adjacent cells or regions, especially in areas where there might be abrupt changes or noise in the data. This can be useful for improving the stability and accuracy of numerical simulations, particularly in cases where sharp discontinuities or high-frequency fluctuations may introduce numerical instabilities or undesirable artifacts.

By applying the filter with a radius equal to the cell size of the mesh, then it is likely that the filter is a low-pass filter. In the context of optimization algorithms, a low-pass filter is commonly used to smooth the results obtained from the optimization process. The filter applies a weighting factor to the objective function values of neighbouring points in the parameter space to obtain a smoothed objective function value. This helps to prevent the optimization algorithm from getting stuck in local minima and improves its ability to converge to the global minimum.

If the amplitude of the filtering is smaller than the cell size, it means that the filter will have a smaller spatial extent compared to the size of the cells in the mesh. This can lead to a more localized smoothing effect, where the filter only affects a smaller number of neighbouring cells around each cell. Consequently, the impact of the filter on the overall smoothing or averaging of the scalar field will be limited to a smaller region of the domain.

The filter, on the other hand, will have a wider spatial extent relative to the size of the cells in the mesh if the amplitude of filtering is higher than the cell size. This might result in excessive smoothing of the data, which could cause the loss of crucial features and information [11][12]. As a result, it's essential to select a filter radius that strikes a compromise between the necessary level of smoothing and the necessity to preserve key data points.

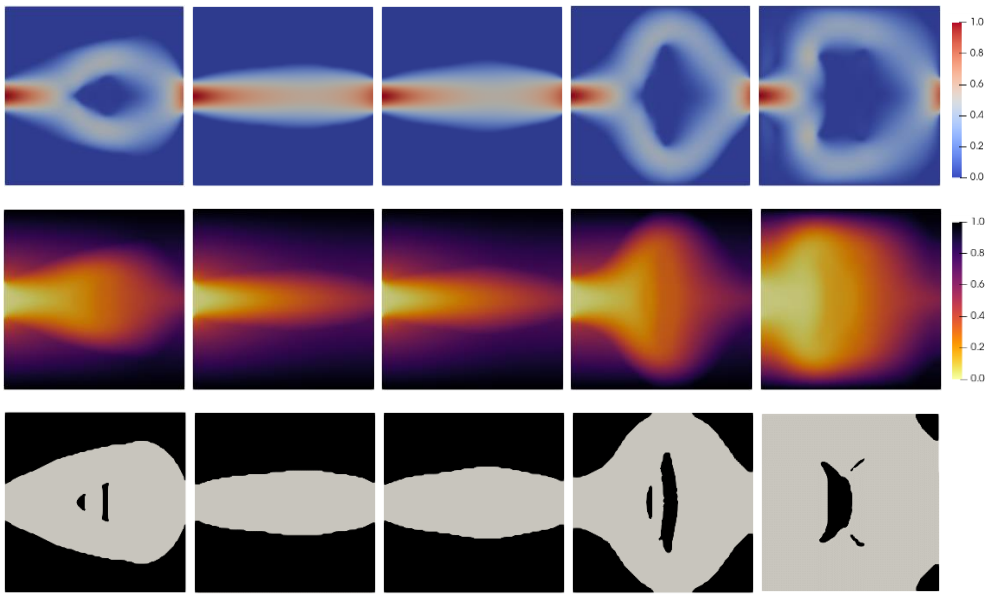

$f = 0.00$ $f = 0.0005$ $f = 0.001$ $f = 0.002$ $f = 0.005$

Figure 13: Normalized velocity, temperature and topology contour plots corresponding to $w = 0.5$ *and* $D = 9.75 \cdot 10^{-5}\ m^2 s^{-1}$ *for different filter widths.*

The choice of filter width determines the level of detail captured in the simulations. As shown in Figure 13, a larger filter width leads to a flow that tends to deflect towards the hot walls (so the recoverable energy transfer should be increased), thus adding material to the centre of the cavity. On the contrary, a smaller filter width captures more details of the flow, however what can be observed is that the flow tends to be straighter, streamlined, without deviations, so a reduction in the mechanical power dissipated should be observed.

It is curious how two clearly marked trends can be observed. On the one hand, a filter size smaller than the cell size tends to centralise the flow, however, as the amplitude increases above the cell size, the tendency is to divert the flow towards the hot walls. This behaviour is similar to that shown when varying the weighting factor, where as the weighting factor is increased the flow was more centralised and streamlined. Thus, the existence of such an analogy can be observed.

Regarding the same results but with the lower thermal diffusivity solid, it can be seen in Figure 14 how the results are practically the same, preserving the original tendency to divert the flow considerably towards the hot walls. Thus, it can be considered that for lower thermal diffusivities, the effect of varying the amplitude of the filter is practically null, since it can be observed that the topological changes in the cavity tend to be the same for any type of amplitude, whether it is greater, smaller or equal to the cell size.

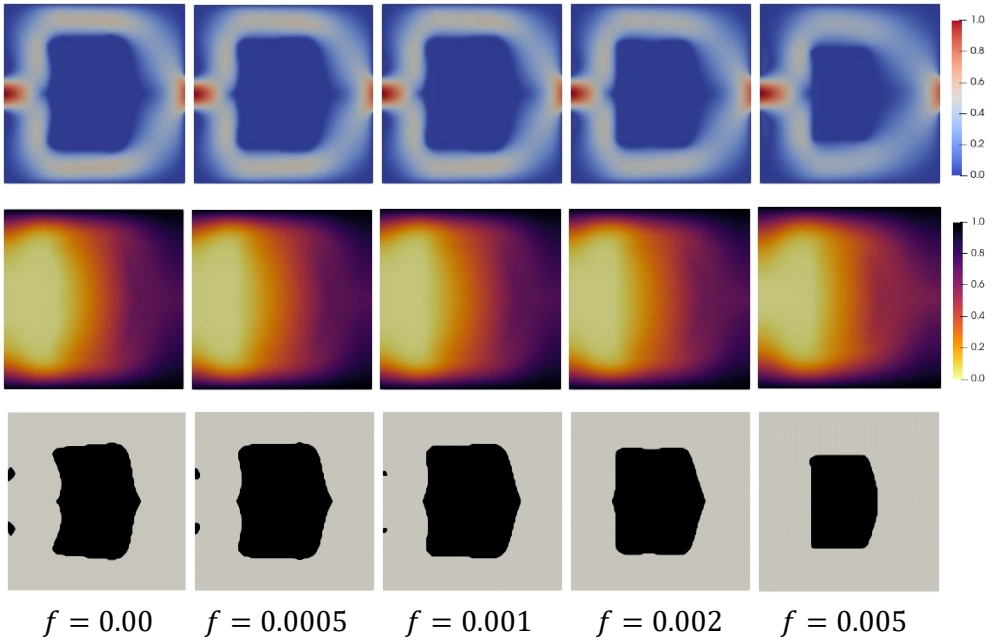

Figure 14: Normalized velocity, temperature and topology contour plots corresponding to $w = 0.5$ *and* $D = 2.1 \cdot 10^{-6}\ m^2 s^{-1}$ *for different filter widths.*

As an additional comment, it is worth noting that the balance between mechanical dissipated power and thermal recoverable energy may depend on other factors and aspects of the simulation setup. However, with a filter amplitude equal to the cell size, it can be expected a reasonable compromise between the two objective functions. The filtering will help in reducing excessive dissipation by smoothing the flow and minimizing small-scale fluctuations while maintaining an adequate level of thermal energy extraction by retaining larger-scale features.

Next, the focus will be on the quantitative aspects of the objective functions, building upon the previous discussions on the characteristics of the velocity, temperature, and topology fields.

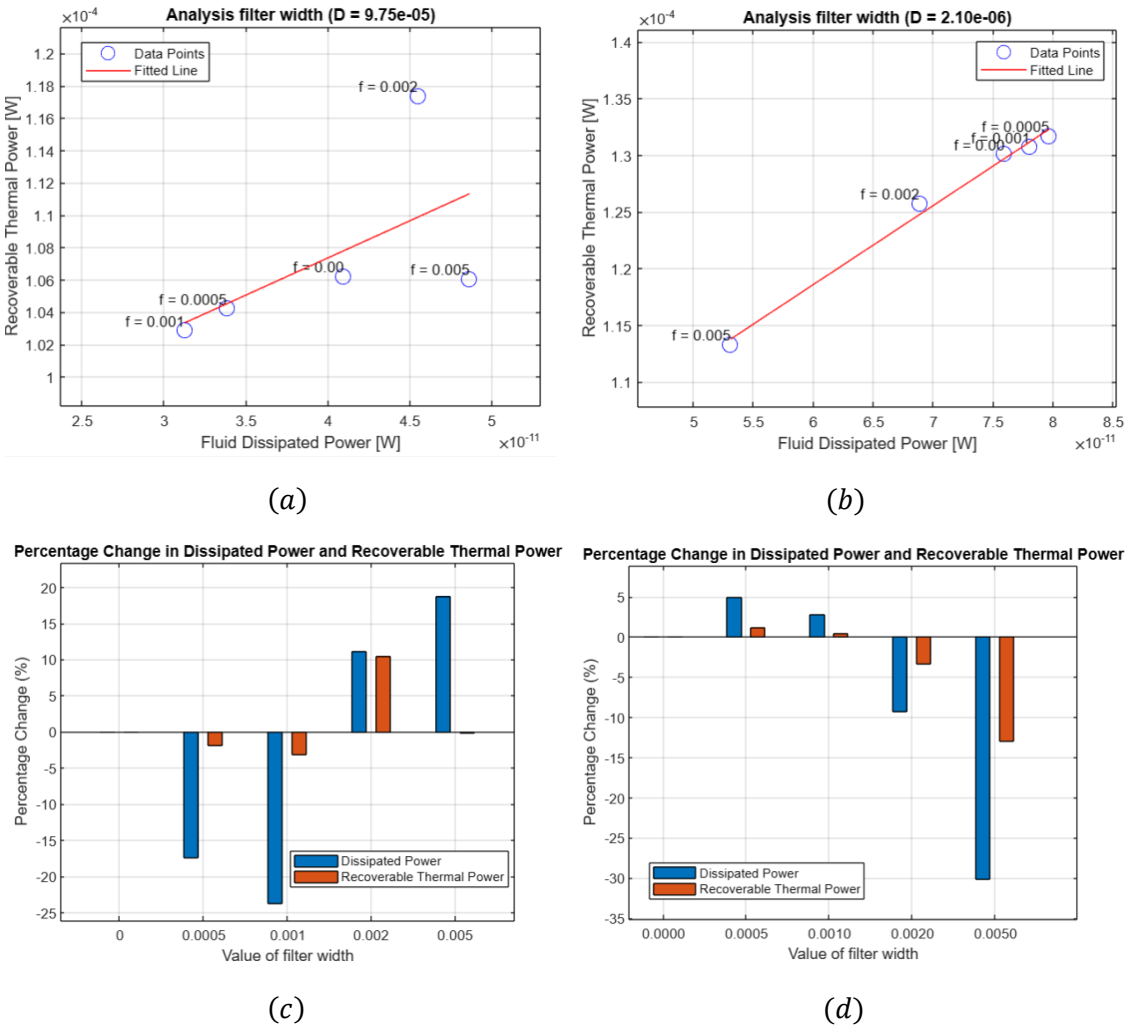

Figure 15: Evolution of the impact on the recoverable thermal power and mechanical dissipated power and bar graphs which account for the percentage change of both objective functions with respect to the base case ($f = 0.00$) for different values of the filter width and different thermal diffusivities: (a)&(c) $D = 9.75 \cdot 10^{-5}\ m^2 s^{-1}$ and (b)&(d) $D = 2.1 \cdot 10^{-6}\ m^2 s^{-1}$.

Figure 15 shows graphs representing the evolution and change in the variables for both objective functions. Analysing first the graph (a), it can be seen how its evolution does not behave in a very linear way compared to graph (b), in which a perfectly linear behaviour can be observed. Analysing the results more closely, it can be appreciated that there is a point of inflection for the filter amplitude very close to the cell size. This can be better appreciated in the bar graphs (c) & (d) where for example in case (c), for amplitudes smaller than the cell size, a decrease of the mechanical power dissipated can be observed while maintaining practically constant the recoverable thermal power (which can be considered beneficial). On the other hand, as the amplitude increases above the cell size, a completely opposite behaviour is observed, increasing the mechanical dissipated power and the recoverable thermal power. This outcome was to be expected, as previously demonstrated, for f values smaller than 0.001, the flow tended to be straight and streamlined, thus decreasing disturbances and consequently reducing mechanical power losses. Similarly, as depicted in Figure 13, for $f > 0.001$, the flow deviated towards the hot walls, thereby increasing the dissipated mechanical power and improving the thermal behaviour.

On the other hand, for the case with lower thermal diffusivity, we have observed that the flow field does not vary significantly. However, quantitatively, some variations in the values of the objective functions can be appreciated in (d). The behaviour is similar, with the appearance of

an inflection point and two opposite trends for f values smaller and larger than the cell size. However, these trends are opposite to those observed in the case of (a) & (c). Now, for $f < 0.001$, the dissipated mechanical power and the thermal recoverable power increase, while for $f > 0.001$, they decrease.

5. Conclusions

In this project, a comprehensive analysis of various parameters and techniques that influence the performance of cooling systems has been conducted. The objective of this research was to gain insights into the optimization process, understand the impact of thermal properties, and explore the effects of smoothing and filtering in computational simulations. The findings presented herein provide valuable knowledge and contribute to the field of cooling system design.

Through the optimization process, it has been observed that the trade-off between mechanical power dissipation and recoverable thermal power is influenced by the weighting factors assigned to each objective function. Increasing the weighting factor for recoverable thermal power leads to significant improvements in harnessing and utilizing heat energy within the system. However, it has been also identified a point of diminishing returns, where further prioritization of recoverable thermal power does not result in substantial reductions in fluid dissipated power. These observations highlight the importance of carefully balancing the objectives during the optimization process.

The RAMP interpolation method, a widely used technique in cooling system simulations, has been thoroughly examined. The role of the k coefficient in regulating the steepness of the interpolation function has been established. Lower values of k result in gentler and smoother transitions, reducing sensitivity to changes in input data. However, caution must be exercised when setting extremely low values of k, as they can increase dissipated power more than recoverable thermal power. Additionally, the influence of the k coefficient on simulation results is more pronounced in cases with reduced thermal diffusivity.

Smoothing and filtering techniques have been explored as means to enhance the accuracy and stability of computational simulations. By adjusting the amplitude or filter width, we can control the level of smoothing applied to the scalar field. It has been observed that. It has been observed that that the filter width actually has a big impact on the simulation results, both in terms of flow field characteristics and in terms of the qualitative results of the objective functions. Striking a balance between necessary smoothing and preserving key data points is vital in achieving optimal results. Furthermore, it has been determined that the influence of the filter amplitude on simulation outcomes is not actually strongly affected when the thermal diffusivity is lowered.

In conclusion, this thesis has provided valuable insights into the optimization process, the utilization of the RAMP interpolation method, and the effects of smoothing and filtering in cooling system simulations. The findings underscore the importance of considering weighting factors, interpolation parameters, and filter widths when designing and optimizing cooling systems. This research contributes to the body of knowledge in the field and provides practical guidance for improving the performance and efficiency of cooling systems. Further studies can build upon these findings to address additional factors and optimize cooling systems in diverse applications.

Bibliography

[1] Gallorini, E., Hèlie, J., & Piscaglia, F. An Adjoint-Based Solver with Adaptive Mesh Refinement For Efficient Design of Coupled Thermal-Fluid Systems. *In Proceedings of the International Conference on Computational Fluid Dynamics.*

[2] Bendsoe, M. P., Kikuchi, N. (1998). Generating optimal topologies in structural design using a homogenization method. *Comput. Methods Appl. Mech. Eng.* Link: Generating optimal topologies in structural design using a homogenization method - ScienceDirect

[3] Bendsoe, M., Sigmund, O. (2004). Topology Optimization: Theory, Methods, and Applications.

[4] Kontoleontos, E. A., Papoutsis-Kiachagias, E. M, A. Zymaris, S., Papadimitriou, D. I. , Giannakoglou, K. C. (2013). Adjoint-based constrained topology optimization for viscous flows, including heat transfer. Link: Adjoint-based constrained topology optimization for viscous flows, including heat transfer: Engineering Optimization: Vol 45, No 8 (tandfonline.com)

[5] Kenway, G.K.W., Mader, C.A., He, P., & Martins, J.R.R.A. (2019). Effective adjoint approaches for computational fluid dynamics. *Progress in Aerospace Sciences.* Doi: Effective adjoint approaches for computational fluid dynamics - ScienceDirect

[6] Patankar, S. V. (1980). Numerical heat transfer and fluid flow. *Hemisphere Publishing Corporation.*

[7] Stolpe M, Svanberg K. (2001). An alternative interpolation scheme for minimum compliance topology optimization. *Structural and Multidisciplinary Optimization.* Link: An alternative interpolation scheme for minimum compliance topology optimization | SpringerLink

[8] Czerwiński, G., Wołoszyn, J. (2021) .Optimization of Air-Cooling System Using Adjoint Solver Technique. Energies, 14, 3753. Doi: 10.3390/en14133753

[9] Kever, N. (2023). Topology Optimization in OpenFOAM using a Continuous Adjoint Framework. *Master thesis, Escola Tècnica Superior d'Enginyeria de Camins, Canals i Ports de Barcelona*. Link: TFM_Kever_Nadeem.pdf (upc.edu)

[10] Ruberto, E. (2017). An adjoint based topology optimization for flows including heat transfer. *Tesi di Laurea Magistrale, Politecnico di Milano, Scuola di Ingegneria Industriale e dell'Informazione, Corso di Laurea Magistrale in Ingegneria Aeronáutica.* Link: 2017_12_Ruberto.pdf (polimi.it)

[11] Sartor, G. (2020). The impact of algorithms for online content filtering or moderation. *European University Institute of Florence, Policy Department for Citizens' Rights and Constitutional Affairs, Directorate-General for Internal Policies.* Link: https://www.europarl.europa.eu/RegData/etudes/STUD/2020/657101/IPOL_STU(2020)657101_EN.pdf

[12] Beechook, A., Fadhila H., Medina J. M., Aleksandrova S. (2017). Effect of grid-filter width definition on implicitly filtered large eddy simulations using OpenFOAM. *Conference paper.* Doi: 10.1063/1.4992186

[13] Qianlong Liu, Oleg V. Vasilyev. (2007). A Brinkman penalization method for compressible flows in complex geometries. *Journal of Computational Physics*. Volume 272, Issue 2. Doi: A Brinkman penalization method for compressible flows in complex geometries | Journal of Computational Physics (acm.org)